Journal of Magnetic Resonance **141,** 164–179 (1999)
Article ID jmre.1999.1859, available online at http://www.idealibrary.com on IDEAL®

Off-Resonance Multiple-Pulse Dynamics in Solid-State NMR Spectroscopy: A Revised Coherent Averaging Theory Analysis

Herman Cho

Environmental Molecular Sciences Laboratory MS K8-98, Pacific Northwest National Laboratory, P.O. Box 999, Richland, Washington 99352

E-mail: hm.cho@pnl.gov

Received May 25, 1999

The standard coherent averaging theory treatment of the resonance offset interaction is compared to exact calculations for multiple-pulse solid-state NMR experiments. Significant differences between coherent averaging approximations and exact results are revealed, even for idealized conditions. A revision of the standard analysis is proposed as a way of improving the description of the off-resonance dynamics in these experiments. We use the insights obtained from this investigation to derive a qualitatively new type of homonuclear decoupling sequence, and evaluate the performance and advantages of this sequence with both simulations and experimental tests.

Key Words: **coherent averaging theory; homonuclear decoupling; multiple-pulse dynamics; solid-state NMR.**

INTRODUCTION

Coherent averaging theory was first conceived by Haeberlen and Waugh (*1, 2*) to analyze the dynamics of homonuclear spin systems in solids during multiple-pulse NMR experiments. In the treatment they proposed, the rotating-frame Hamiltonian was assumed to be the sum of a time-independent term V, consisting of interactions of the spins with internal magnetic fields, and a time-dependent, piecewise constant term, $\mathcal{H}_1(t)$, representing the interaction of the spins with modulated radiofrequency (rf) fields generated by the experimental apparatus:

$$\mathcal{H}(t) = \mathcal{H}_1(t) + V. \qquad [1]$$

At the end of a periodically repeated decoupling sequence of cycle time T, the state of a system with this Hamiltonian is determined by the time development operator $U(T)$, which, according to coherent averaging theory, can be written

$$U(T) = U_1(T)U_V(T), \qquad [2]$$

with

$$U_1(t) = \vec{\mathcal{T}}\ \exp\left\{-i\int_0^t \mathcal{H}_1(t')dt'\right\}, \qquad [3]$$

$$U_V(t) = \vec{\mathcal{T}}\ \exp\left\{-i\int_0^t \tilde{V}(t')dt'\right\}, \qquad [4]$$

where $\vec{\mathcal{T}}$ is the Dyson time ordering operator (*3*) and $\tilde{V}(t)$ is the internal Hamiltonian in the so-called toggling frame (*2*):

$$\tilde{V}(t) = U_1^{-1}(t)VU_1(t). \qquad [5]$$

An exact expression for $U_1(T)$ can usually be obtained, but not so for $U_V(T)$. In a coherent averaging theory approach, a form for $U_V(T)$ is found by applying

$$U_V(T) = \exp\{-i\bar{V}T\}, \qquad [6]$$

where $\bar{V}$ is a time-independent "effective" Hamiltonian that is approximated by truncating the Magnus expansion (*2, 4*) of $\tilde{V}(t)$.

Haeberlen and Waugh were originally concerned with internal Hamiltonians V containing two types of interactions: the homonuclear dipolar coupling and the effective resonance offset interaction, described by the Hamiltonians $\mathcal{H}_d$ and $\mathcal{H}_\delta$, respectively. The coherent averaging theory analysis of the second of these interactions is the focus of this paper (*5*). This investigation is motivated by a recent report revealing large discrepancies between exact calculations and the standard coherent averaging theory description of the off-resonance dynamics in multiple-pulse NMR experiments (*6*). In examining the results of a multiple-pulse decoupling experiment, accurate evaluations of the effective resonance offset Hamiltonian $\bar{\mathcal{H}}_\delta$ and cross terms involving $\mathcal{H}_\delta$ are desired for several reasons. The first is that the frequency dependence of $\bar{\mathcal{H}}_\delta$ must be

1090-7807/99 $30.00

TABLE 1
Multiple-Pulse Homonuclear Decoupling Sequences and Corresponding Resonance Offset Hamiltonians

Name	Pulse sequence[a]	$\bar{\mathcal{H}}_\delta^{(0)b}$	Precession axis[b]	Offset scale factor[b]
WAHUHA (*20*)	$(X\bar{Y})(Y\bar{X})$	$\frac{1}{3}\sum_{j=1}^{N}\delta_j(I_{xj}+I_{yj}+I_{zj})$	$\frac{1}{\sqrt{3}}(1,1,1)$	$\frac{1}{\sqrt{3}}$
MREV-8 (*8, 28–30*)	$(X\bar{Y})(Y\bar{X})(\bar{X}\bar{Y})(YX)$	$\frac{1}{3}\sum_{j=1}^{N}\delta_j(I_{xj}+I_{zj})$	$\frac{1}{\sqrt{2}}(1,0,1)$	$\frac{\sqrt{2}}{3}$
BR-24 (*14*)	$(\bar{Y}X)(\bar{X}Y)(YX)(\bar{X}\bar{Y})$ $(X\bar{Y})(Y\bar{X})(\bar{X}\bar{Y})(X\bar{Y})$ $(Y\bar{X})(\bar{X}\bar{Y})(YX)(YX)$	$\frac{2}{9}\sum_{j=1}^{N}\delta_j(I_{xj}+I_{yj}+I_{zsj})$	$\frac{1}{\sqrt{3}}(1,1,1)$	$\frac{2}{3\sqrt{3}}$

[a] Sequences specified according to the scheme of Burum and Rhim (*14*).
[b] Zeroth-order coherent averaging theory values, neglecting finite pulse widths.

known in order to relate the spectra measured by multiple-pulse techniques to the chemical shifts of the sample. Typically, multiple-phase spectra are interpreted according to zeroth-order coherent averaging theory, which predicts that the observed frequencies are equal to the resonance offsets contained in $\mathcal{H}_\delta$ multiplied by a constant scale factor characteristic of the multiple-phase sequence (*2, 7*). If $\bar{\mathcal{H}}_\delta$ contains large higher order terms, however, then chemical shift spectra derived on the basis of zeroth-order assumptions will contain systematic, nonlinear errors. The magnitude of this error is quantified in later sections.

The second purpose for investigating the approximation of $\bar{\mathcal{H}}_\delta$ is to find explanations and remedies for the distortions and artifacts that afflict multiple-pulse spectra, such as carrier-frequency and image lines (*2, 6, 8–11*). Strategies for eliminating these unwanted effects have been proposed in the past, but have not been entirely successful, due mainly to deviations from idealized zeroth-order behavior (*6*). These effects are especially troublesome in multiple-pulse spectra with several lines dispersed over large bandwidths.

Our final reason for examining off-resonance multiple-pulse dynamics is to elucidate the off-resonance line-narrowing performance of homonuclear decoupling sequences. Several workers, including Haeberlen *et al.* (*12*), Pines and Waugh (*13*), Rhim *et al.* (*8, 14*), and Garroway *et al.* (*15*), have studied the effects of the resonance offset on the performance of early multiple-pulse sequences, especially with regard to resolution. The standard treatment, as developed in this past work, has been to include higher order Magnus expansion terms in the approximation of $\bar{V}$. Such calculations are feasible for short sequences, but in general the evaluation and interpretation of Magnus expansion terms beyond second order, particularly cross terms, can be prohibitively complex, and are of limited utility. A different approach that did not require the evaluation of higher order terms would be preferable, both for analyzing existing experiments and for developing improved new ones.

In this paper, we propose an alternative to the standard toggling frame as the starting point for a revised coherent averaging theory analysis of multiple-pulse dynamics. We show that for the best known of the homonuclear multiple-pulse sequences, there is an interaction representation distinct from the toggling frame, which in important respects represents a superior frame of reference for the treatment of multiple-pulse dynamics. The insights on the dynamics obtained in this new interaction representation are used to derive a qualitatively new homonuclear decoupling sequence with characteristics that in certain circumstances are superior to any other sequence proposed to date.

THEORY

Comparison of Coherent Averaging Theory with Exact Calculations

In this section, we compare standard toggling-frame coherent averaging theory approximations with exact results for a simple spin system. Throughout this paper, we shall consider only homonuclear collections of spin-$\frac{1}{2}$ particles in rigid solids.

To isolate the action of the resonance offset on the spin dynamics, we specify a single-spin rotating-frame Hamiltonian V consisting only of a resonance offset term. Zeroth-order Magnus expansion approximations of the toggling-frame resonance offset Hamiltonians for three multiple-pulse experiments are gathered in Table 1. We will assume that the effects of the resonance offset can be neglected during rf pulses, as expressed by the equations

$$\begin{aligned} \mathcal{H}(t) &= \delta I_z \quad \text{during free evolution,} \\ \mathcal{H}(t) &= \omega_1(\cos\phi I_x + \sin\phi I_y) \quad \text{during pulse of phase } \phi, \end{aligned} \tag{7}$$

where we have adopted the usual definition of the rotating-frame z-axis as the direction collinear with the applied magnetic field, δ is the offset of the rf carrier from the resonance frequency of the spin, and ω_1 is the rf field amplitude in radians s^{-1}.

Any motion of an isolated spin-$\frac{1}{2}$ particle can be represented as a rotation in a three-dimensional Cartesian space (*16, 17*).

With the Hamiltonians as given in Eq. [7], the rotation corresponding to periods of free evolution is about the z-axis through the angle δt, where t is the duration of the free evolution period. The motion corresponding to evolution during a rf pulse of duration t_p is described by a rotation about the rotating-frame axis ($\cos\phi$, $\sin\phi$, 0) through an angle $\omega_1 t_p$. We write the mathematical operators corresponding to these rotations in the form $R_\alpha(\psi)$, where α is the axis of the rotation (i.e., $\pm x$, $\pm y$, $\pm z$) and ψ equals the angle of the rotation.

The equivalence of the motion to simple rotations implies that the evolution during a multiple-pulse sequence can be represented as a product of rotation operators. For the four-pulse WAHUHA sequence, this product is

$$R_{\mathbf{r}}(\psi) = R_z(\delta\tau_e)\,R_{\bar{x}}(\pi/2)\,R_z(\delta\tau_s)\,R_y(\pi/2)\,R_z(\delta\tau_l) \times R_{\bar{y}}(\pi/2)\,R_z(\delta\tau_s)\,R_x(\pi/2)\,R_z(\delta\tau_b), \quad [8]$$

with the idealized free evolution times τ_s, τ_l, τ_b, and τ_e satisfying the relations

$$\tau_l = 2\tau_s, \quad [9]$$

$$\tau_l = \tau_b + \tau_e, \quad [10]$$

$$T = 6\tau_s. \quad [11]$$

The time τ_b is the duration of the period preceding the first pulse of the sequence, τ_e is the duration of the period following the last pulse of the sequence, and T denotes the cycle time of the sequence. The vector $\mathbf{r}$ is the normalized precession axis of the product rotation, which we specify with the spherical polar longitudinal and azimuthal angles β and γ, respectively.

Given δ, τ_s, and τ_e, the parameters ψ and $\mathbf{r}$ can be computed exactly (*18*) and the true offset scaling factor in the ideal pulse limit calculated from ψ via the definition

$$S \equiv \left|\frac{\psi}{\delta T}\right|. \quad [12]$$

The results of such a calculation are shown in Fig. 1 for the WAHUHA, MREV-8, and BR-24 sequences. In each case, the offset range is limited by the Nyquist sampling theorem (*19*) to values within the bounds $\pi/S \geq |\delta T|$, with S taken from the zeroth-order coherent averaging theory data in Table 1.

The discrepancy between the exact result and the coherent averaging theory calculation is considerably reduced by adding the first- and second-order Magnus expansion corrections to the zeroth-order expression. The plots in Fig. 2 illustrate the improvement when these terms are included for the WAHUHA sequence. The effective offset Hamiltonian evaluated to second order has been reported for WAHUHA in the ideal pulse limit where $\tau_b = \tau_e = \tau_s$ (*2*); we have rederived these higher order terms not assuming that $\tau_b = \tau_e$, with the results

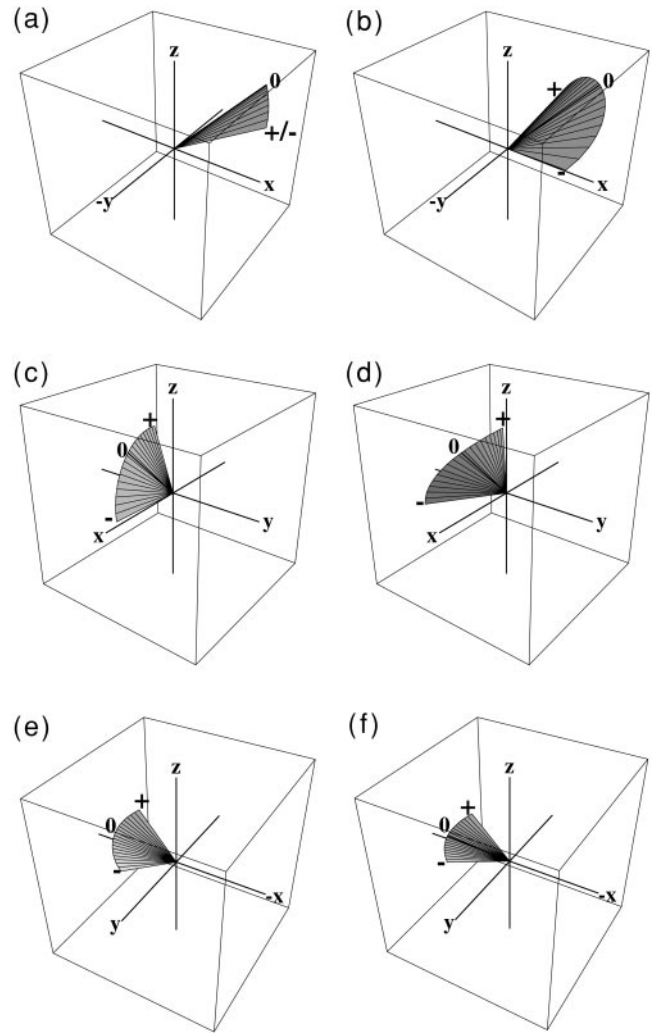

FIG. 1. Effective precession axes as a function of resonance offset for WAHUHA (a, b), MREV-8 (c, d), and BR-24 (e, f) sequences. The fan-shaped surfaces are exact results for $\tau_b = \tau_e = \tau_s$ (a, c, e) and $\tau_b = 0$, $\tau_e = 2\tau_s$ (b, d, f), evaluated over the range $7\pi/4 \geq |\delta T|$ (WAHUHA), $2\pi \geq |\delta T|$ (MREV-8), and $5\pi/2 \geq |\delta T|$ (BR-24). The vectors forming the surfaces represent the directions of the precession axes drawn from the origin, with lengths proportional to the true scaling factor S. The (−) and (+) symbols indicate the direction of increasing δT. The only resonance offset value where the zeroth-order predictions from Table 1 and the exact result coincide is $\delta = 0$, marked as 0. The separation between adjacent lines on the surfaces represents 1/19 of the Nyquist theorem-limited δT range.

$$\bar{\mathcal{H}}_\delta^{(1)} = \frac{\delta^2}{6}(\tau_b - \tau_e)(I_x - I_y), \quad [13]$$

$$\bar{\mathcal{H}}_\delta^{(2)} = \frac{\delta^3}{18}[(2\tau_b\tau_e - \tau_b^2 + 2\tau_b\tau_s - \tau_s^2)I_x + (2\tau_b\tau_e - \tau_b^2 + 2\tau_b\tau_s - 4\tau_s^2)I_y - 2\tau_s(\tau_b + \tau_e)I_z]. \quad [14]$$

The zeroth-order term is unchanged.

The symmetry of the left series of curves in Fig. 2 represents

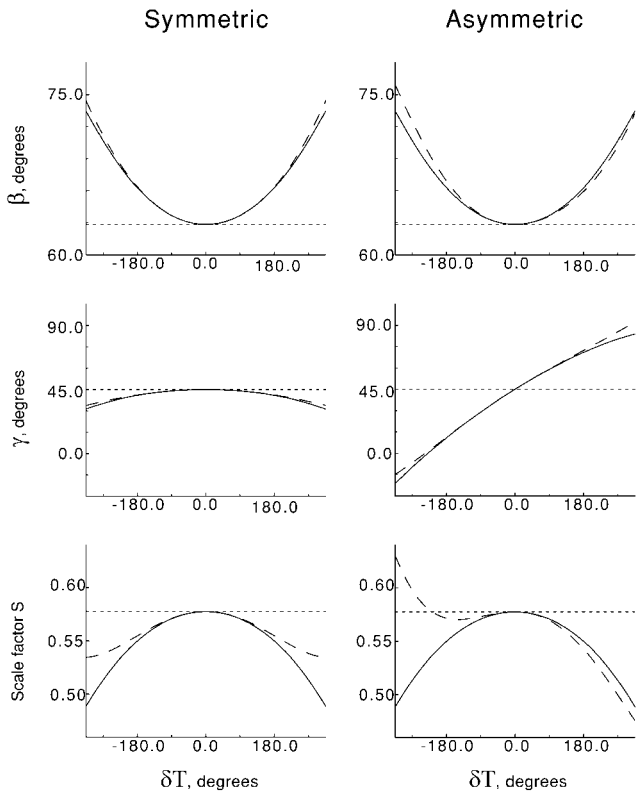

FIG. 2. WAHUHA precession axis parameters as functions of resonance offset for an isolated spin-$\frac{1}{2}$ nucleus, with $\tau_b = \tau_e = \tau_s$ (left) and $\tau_b = 0$, $\tau_e = 2\tau_s$ (right). The three curves in each plot represent the exact result (solid curve), the zeroth-order coherent averaging theory result (horizontal dotted line), and the coherent averaging theory result calculated to third (left) or second (right) order (dashed curve). The offset from the carrier frequency is designated on the abscissa as a product with the sequence cycle time, δT, evaluated over the range $-315° \leq \delta T \leq 315°$.

a notable contrast to the right series, and is a manifestation of the underlying symmetry of the toggling-frame offset Hamiltonian. The toggling-frame offset Hamiltonian (which we denote $\tilde{\mathcal{H}}_\delta(t)$) for the version of WAHUHA with $\tau_b = \tau_e = \tau_s$, is symmetric in the sense that $\tilde{\mathcal{H}}_\delta(t) = \tilde{\mathcal{H}}_\delta(T - t)$. Wang and Ramshaw (*21*) have shown that for Hamiltonians with this property, all odd-order terms of the Magnus expansion are identically zero. It follows that the effective offset Hamiltonian must be an odd function of the offset frequency to all orders, and the scale factor and effective precession axis coordinates must be even functions of the offset frequency to all orders. For sequences with an asymmetry introduced by, e.g., specifying unequal values for τ_b and τ_e, odd-order terms of the Magnus expansion of the toggling-frame Hamiltonian will not be zero, and the precession axis coordinates will no longer necessarily be even functions of the offset frequency. The γ vs δT curves in the right series, for which $\tau_b \neq \tau_e$, display the appearance of this asymmetry. The curves for the exact calculation of β vs δT and S vs δT in the right series, however, are even functions of the offset frequency, the asymmetry of $\tilde{\mathcal{H}}_\delta(t)$ notwithstanding. In fact, the exact calculations of the β and S curves for the case where $\tau_b \neq \tau_e$ (right series) are identical to the exact β and S curves for the symmetric case where $\tau_b = \tau_e$ (left series). A proof of this assertion is given in Appendix A. This assertion does not necessarily apply if $\bar{V}$ is approximated by a truncated Magnus expansion. Because $\bar{\mathcal{H}}_\delta^{(1)}$ is nonzero when $\tau_b \neq \tau_e$, the second-order coherent averaging theory expressions for γ, β, and S will contain some odd component, which is observed.

Approximations of $\bar{\mathcal{H}}_d$ and $\bar{\mathcal{H}}_\delta$

The validity of approximating $\bar{\mathcal{H}}_d$ with a Magnus expansion of the toggling-frame homonuclear dipolar Hamiltonian $\tilde{\mathcal{H}}_d(t)$, truncated to low orders, has been confirmed by both experimental and mathematical investigations (*1, 2, 7, 22–27*). The ultimate resolution in most circumstances is determined by the largest of the nonzero terms in the Magnus expansion, which are typically higher order cross terms involving the dipolar Hamiltonain $\mathcal{H}_d$ (*2, 7, 8, 14, 15, 28–33*). Nonetheless, *zeroth-order* coherent averaging theory alone is a valuable way to analyze the decoupling performance of these sequences, even when higher order terms are not zero.

At first glance, therefore, the finding that $\bar{\mathcal{H}}_\delta$ deviates significantly from the zeroth-order Magnus expansion term $\bar{\mathcal{H}}_\delta^{(0)}$ appears to be contradicted by the success of the zeroth-order approximation in modeling $\bar{\mathcal{H}}_d$. Since resonance offsets are typically smaller than homonuclear dipolar interactions, we might expect better, not worse, agreement between zeroth-order resonance offset calculations and the exact results.

There is no inconsistency, however, in the conclusion that the zeroth-order coherent averaging theory approximation is accurate for $\bar{\mathcal{H}}_d$, but inaccurate for $\bar{\mathcal{H}}_\delta$. As Haeberlen has shown (*2*), for decoupling sequences constructed from "solid echo pulse groups" (*14*), higher order Magnus expansion dipolar terms are small and $\bar{\mathcal{H}}_d \approx \bar{\mathcal{H}}_d^{(0)} = 0$, provided that the window lengths are short compared to the inverse root of the second moment of the dipolar-broadened linewidth. Since this criterion is usually satisfied, $\bar{\mathcal{H}}_d^{(0)}$ is an accurate approximation of $\bar{\mathcal{H}}_d$ over both short and long timescales for this particular class of multiple-pulse sequences.

The resonance offset interaction on the other hand is not suppressed during a multiple-pulse sequence and $\bar{\mathcal{H}}_\delta^{(0)} \neq 0$. Indeed, the usual objective is to maximize $\bar{\mathcal{H}}_\delta^{(0)}$ in order to improve spectral dispersion. The evolution of the spin system due to this interaction accumulates during the sequence, and higher order nonlinear Magnus expansion terms become critical in approximating $\bar{\mathcal{H}}_\delta$.

Modifications of the Coherent Averaging Theory Approach

The analysis above implies that the time average alone of $\tilde{\mathcal{H}}_\delta(t)$ in the toggling frame, i.e., $\bar{\mathcal{H}}_\delta^{(0)}$, is a questionable approximation of $\bar{\mathcal{H}}_\delta$. It is natural to inquire if there is another interaction representation that would lead to a more satisfactory and tractable treatment of the off-resonance dynamics.

The choice of interaction representation is determined by the definition of $\mathcal{H}_1(t)$. The customary definition is $\mathcal{H}_1(t) \equiv \mathcal{H}_{rf}(t)$, where $\mathcal{H}_{rf}(t)$ is the Hamiltonian corresponding to the Zeeman interaction of the spins with the rf fields. This implies the following form for the multispin internal Hamiltonian V:

$$V = \mathcal{H}_d + \mathcal{H}_\delta, \quad [15]$$

$$\mathcal{H}_d = \frac{1}{2} \sum_{\substack{j,k=1 \\ j \neq k}}^{N} d_{jk}(3I_{zj}I_{zk} - \mathbf{I}_j \cdot \mathbf{I}_k), \quad [16]$$

$$\mathcal{H}_\delta = \sum_{j=1}^{N} \delta_j I_{zj}. \quad [17]$$

An alternative to the toggling frame is suggested by Eq. [8]. The alternative we consider is defined by the relations

$$\mathcal{H}_1(t) \equiv \mathcal{H}_{rf}(t) + \mathcal{H}_\delta, \quad [18]$$

$$V = \mathcal{H}_d. \quad [19]$$

The influence of the resonance offset interaction on the evolution of the spin system is treated exactly in this new frame, and the troublesome approximation of $\bar{\mathcal{H}}_\delta$ by truncated Magnus expansions is avoided. We call this new interaction representation the "offset-toggled frame."

A number of the key features of this approach can be appreciated by analyzing the two-pulse solid echo sequence τ_1–$(\frac{\pi}{2})_x$–τ_2–$(\frac{\pi}{2})_{\bar{y}}$–$\tau_3$ in the offset-toggled frame. The solid echo sequence is the basic unit of virtually every homonuclear decoupling sequence developed to date, and the properties of longer sequences are largely derived from this unit (*14*). We simplify the calculations by assuming that $\omega_1 \gg \delta_j$ for all spins, and

$$\mathcal{H}_1(t) = \sum_{j=1}^{N} \delta_j I_{zj} \quad \text{during free evolution,}$$

$$\mathcal{H}_1(t) = \sum_{j=1}^{N} \omega_1(\cos\phi I_{xj} + \sin\phi I_{yj}) \quad \text{during pulse of phase } \phi.$$

Following standard formulas for the Magnus expansion (*2, 4, 7, 22–25*), $\bar{\mathcal{H}}_d^{(0)}$ can be evaluated by piecewise integration of $\mathcal{H}_d(t)$. The result is

$$\bar{\mathcal{H}}_d^{(0)} = \frac{1}{T}[\tau_1\bar{\mathcal{H}}_{d,1}^{(0)} + \tau_2\bar{\mathcal{H}}_{d,2}^{(0)} + \tau_3\bar{\mathcal{H}}_{d,3}^{(0)} + t_p(\bar{\mathcal{H}}_{d,x}^{(0)} + \bar{\mathcal{H}}_{d,\bar{y}}^{(0)})]. \quad [21]$$

$\bar{\mathcal{H}}_{d,1}^{(0)}$, $\bar{\mathcal{H}}_{d,2}^{(0)}$, and $\bar{\mathcal{H}}_{d,3}^{(0)}$ are the contributions to $\bar{\mathcal{H}}_d^{(0)}$ of the three free evolution intervals, and $\bar{\mathcal{H}}_{d,x}^{(0)}$ and $\bar{\mathcal{H}}_{d,\bar{y}}^{(0)}$ are the contributions of the two rf pulse intervals. We have computed $\bar{\mathcal{H}}_{d,x}^{(0)}$ and $\bar{\mathcal{H}}_{d,\bar{y}}^{(0)}$, but the equations are lengthy and we do not reproduce them here. Instead, we make the assumption that t_p is short compared to T and write $\bar{\mathcal{H}}_d^{(0)}$ as

$$\bar{\mathcal{H}}_d^{(0)} = \frac{1}{T}(\tau_1\bar{\mathcal{H}}_{d,1}^{(0)} + \tau_2\bar{\mathcal{H}}_{d,2}^{(0)} + \tau_3\bar{\mathcal{H}}_{d,3}^{(0)}). \quad [22]$$

Expressions for $\bar{\mathcal{H}}_{d,1}^{(0)}$, $\bar{\mathcal{H}}_{d,2}^{(0)}$, and $\bar{\mathcal{H}}_{d,3}^{(0)}$ appear in Appendix B.

Comparison of Interaction Representations

An analysis of multiple-pulse line-narrowing sequences in the toggling frame differs in a number of ways from an analysis in the offset-toggled frame:

1. In the offset-toggled frame, $\tilde{\mathcal{H}}_d(t)$ is not a piecewise constant function of time, even in the ideal pulse limit. Furthermore, sequences for which $\tilde{\mathcal{H}}_d(t)$ is symmetric in the toggling frame (such as WAHUHA) lose their symmetry in the offset-toggled frame, except on resonance.
2. The transformation of $\mathcal{H}_d$ to the offset-toggled frame cannot be described as the rotation of a second-rank irreducible spherical tensor in the ideal pulse limit (*2, 7, 34, 35*). The transformation of $\mathcal{H}_d$ must be treated as a linear operation on a nine-dimensional bilinear Cartesian tensor space.
3. $U_1(t)$ and $\tilde{\mathcal{H}}_d(t)$ in the toggling frame are independent of the offset frequencies of the coupled spins. In the offset-toggled frame, however, both $U_1(t)$ and $\tilde{\mathcal{H}}_d(t)$ (and hence $\bar{\mathcal{H}}_d$) are complicated functions of the δ_i.
4. Because of the dependence of $U_1(t)$ on the offset frequencies, the offset-toggled frame and the rotating frame will not coincide in the observation window except when the offset frequencies of coupled spins are equal to zero.

The derivation of Eq. [22] exemplifies most of these items. Although we were able to obtain an analytical expression for $\bar{\mathcal{H}}_d^{(0)}$ for the solid echo sequence, the calculation quickly grows in complexity as the sequence length increases. Generalizing from Eq. [22], however, we can infer that $\bar{\mathcal{H}}_d^{(0)}$ in the offset-toggled frame *will not equal zero* except for pairs of dipolar-coupled spins that are exactly on resonance.

Despite the difficulties of deriving analytical expressions, it is possible to evaluate $\bar{\mathcal{H}}_d^{(0)}$ numerically. The result would be an equation of the form

$$\bar{\mathcal{H}}_d^{(0)} = \frac{1}{2} \sum_{\substack{j,k=1 \\ j \neq k}}^{N} d_{jk} \sum_{\alpha,\beta}^{x,y,z} A_{\alpha\beta}(\delta_j, \delta_k) I_{\alpha j} I_{\beta k}, \quad [23]$$

where δ_j and δ_k are the resonance offset frequencies of the jth and kth spins, respectively. By analogy with the offset scaling

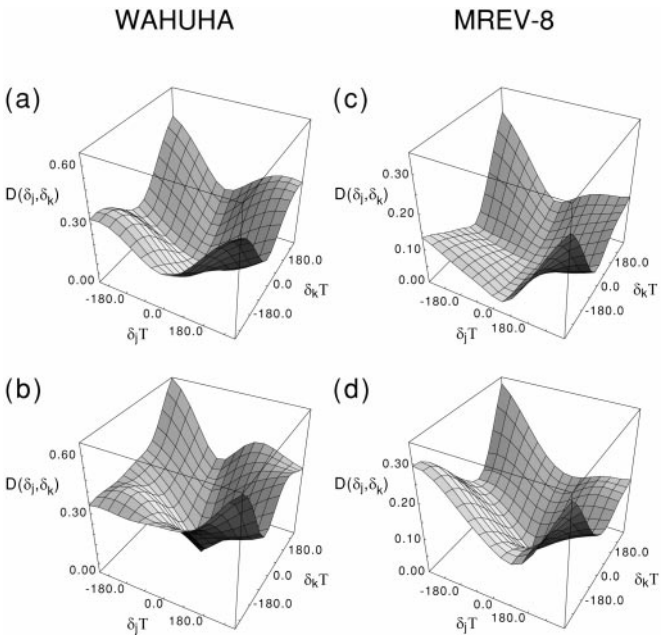

FIG. 3. Dipolar coupling scaling factor $D(\delta_j, \delta_k)$ in the offset-toggled frame, plotted as a function of the resonance offsets of the two dipolar-coupled spins. (a) Symmetrized WAHUHA sequence with $\tau_b = \tau_e = \tau_s$. (b) Asymmetric WAHUHA sequence with $\tau_b = 0$ and $\tau_e = 2\tau_s$. (c) Symmetrized MREV-8 sequence with $\tau_b = \tau_e = \tau_s$. (d) Asymmetric MREV-8 sequence with $\tau_b = 0$ and $\tau_e = 2\tau_s$.

factor S, we define a normalized dipolar coupling constant scaling factor $D(\delta_j, \delta_k)$:

$$D(\delta_j, \delta_k) \equiv 6^{-1/2} [\sum_{\alpha,\beta}^{x,y,z} (A_{\alpha\beta}(\delta_j, \delta_k))^2]^{1/2}. \qquad [24]$$

The factor of $6^{-1/2}$ is required for normalization of the spin operator part of the dipolar coupling Hamiltonian defined by Eq. [2].

$D(\delta_j, \delta_k)$ is a scalar function that can be visualized as a hypersurface above the (δ_j, δ_k) plane. A representative series of these hypersurfaces appears in Fig. 3. These figures illustrate the imperfect performance of line-narrowing sequences away from resonance. Even in zeroth order, the effective bilinear coupling deviates significantly from zero as the carrier frequency is moved off resonance. When the two spins have different chemical shifts, it is effectively impossible to null the apparent homonuclear bilinear couplings with any of these decoupling sequences.

Together with Fig. 2, Fig. 3 also elucidates how the appearance of a multiple-pulse spectrum is affected by the time in the sampling window where the complex data are digitized. For example, noting Fig. 3, one might infer that the midpoint of the sampling window is a better place to acquire data than the end of the window for optimal line narrowing. The variability of the direction of the precession axis as a function of offset frequency is also minimized with this choice of acquisition time.

Early studies of multiple-pulse decoupling sequences (*8, 12, 14, 15*) have demonstrated that line-narrowing performance measurably worsens when the spectrometer carrier frequency is not on resonance. Equation [23] and Fig. 3 symbolize the explanation a zeroth-order calculation in the offset-toggled frame provides for this effect, including the observation that line-narrowing performance depends on the sign of the offset frequency. Unlike the zeroth-order theory in the toggling frame, a zeroth-order analysis in the offset-toggled frame can be used to predict the functional dependence of the resolution on the offset frequencies. At least part of the offset dependence of the spectral resolution is attributable to pulse errors and other instrumental imperfections, which we have not considered. As we shall see in later simulations, however, most major line-broadening phenomena caused by the resonance offset interaction can be accounted for by the zeroth-order theory, as embodied by Eq. [23].

Theoretical models based on a second averaging (*2, 7, 12, 13*) of the dipolar interaction in the toggling frame can in principle account for many of the nonlinear offset-dependent phenomena observed in multiple-pulse decoupling experiments. Nevertheless, an exact analysis of multiple-pulse dynamics in the presence of a resonance offset interaction reveals at least two difficulties with the traditional second averaging approach. The first is that the coordinates of the effective offset precession axis are not independent of the resonance offset, as has been assumed in second averaging treatments. While second averaging calculations can be modified to account for this effect, the results are considerably more complicated than have been previously assumed.

The second difficulty becomes apparent when one considers the situation where dipolar-coupled spins have different chemical shifts. Second averaging analyses, as previously formulated, provide no guidance when coupled spins precess about different effective axes and with different effective frequencies in the observation frame.

Derivation of a New Multiple-Pulse Decoupling Sequence

The nonlinearity of $\bar{\mathcal{H}}_\delta$ in the toggling frame and its attendant complications can be neglected if δT is sufficiently small. The experimental requirement is a spectrometer that can generate decoupling sequences with cycle times T that are short compared to the inverse of the offset frequencies. In fact, the suppression of nonlinear resonance offset dynamics often requires cycle times that are shorter than those needed to ensure that $\bar{\mathcal{H}}_d \approx 0$. Prominent deviations from linear behavior are observed in multiple-pulse spectra, even when the entire chemical shift range occupies no more than the middle 10% of a sequence's Nyquist bandwidth, and rapidly increase as NMR lines move outside this range (*6*).

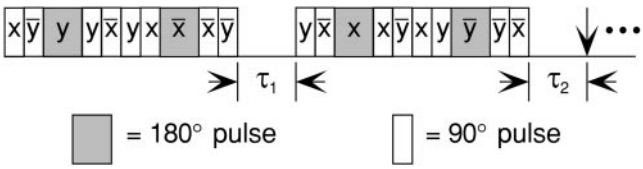

FIG. 4. Pulse phases and timing of the EMSL-30 homonuclear decoupling sequence. One complex datum per EMSL-30 cycle is acquired at the point indicated by the arrow. The sequence duration, including windows, is equal to $30t_p$, with $\tau_1 = \tau_2 = 3t_p$ and $t_p = 90°$ pulse time.

The problems associated with the long cycle times and nonlinear offset effects would be minimized if the toggling-frame resonance offset Hamiltonian $\tilde{\mathcal{H}}_\delta(t)$ commuted with itself at all times. For Hamiltonians $\tilde{\mathcal{H}}_\delta(t)$ that are self-commuting for all t, the only nonzero term in the Magnus expansion would be the linear term, $\bar{\mathcal{H}}_\delta^{(0)}$.

For multiple-pulse decoupling sequences consisting of concatenated solid echo pulse groups, which include virtually every non-windowless sequence developed to date, $\tilde{\mathcal{H}}_\delta(t)$ will not commute with itself in the toggling frame. Also, for most cases of practical interest, the requisite short cycle times are difficult to achieve with current instrumentation; but even if they were not, the duty cycles required, the power deposited in the sample, and the length of the acquisition times would approach undesirably high values. We conclude that the off-resonance dynamics of sequences composed of solid echo pulse groups is highly nonlinear, even if the spectrometer's performance is considered to be ideal.

Based on these observations, we infer two rules to guide the development of improved decoupling sequences using a toggling-frame analysis:

1. It is desirable to have the effective precession axis be parallel to the rotating-frame z-axis (*6*). Spectral artifacts will be reduced and the effective bandwidth of the sequence will double if such a precession axis can be stipulated.
2. Pulses and windows should be arranged so that $\tilde{\mathcal{H}}_\delta(t)$ commutes with itself for all times.

Given the need to ensure that $\bar{\mathcal{H}}_d \approx 0$, the second rule may seem impossible to obey. Higher order Magnus expansion terms that arise because $\tilde{\mathcal{H}}_\delta(t)$ does not commute with itself can nevertheless be minimized by keeping the sequence cycle time short and eliminating windows in the sequence, especially intervals where $\tilde{\mathcal{H}}_\delta(t) \neq \mathcal{H}_\delta$.

Following these principles, we have developed a new multiple-pulse sequence called EMSL-30 (Fig. 4), after the *E*nvironmental *M*olecular *S*ciences *L*aboratory (*36*). The EMSL-30 dipolar and resonance offset zeroth-order Magnus expansion terms in the toggling frame are

$$\bar{\mathcal{H}}_d^{(0)} = 0\,, \qquad [25]$$

$$\bar{\mathcal{H}}_\delta^{(0)} = \frac{1}{5}\left(\frac{8}{3\pi} + 1\right)\mathcal{H}_\delta. \qquad [26]$$

These results were computed by integrating $\tilde{\mathcal{H}}_d(t)$ and $\tilde{\mathcal{H}}_\delta(t)$ during both windows and pulses.

Radiofrequency inhomogeneity can significantly impair the effectiveness of multiple-pulse sequences. This interaction can be modeled by a Hamiltonian of the form

$$\mathcal{H}_\epsilon(t) = 0 \quad \text{during free evolution,}$$

$$\mathcal{H}_\epsilon(t) = \sum_{j=1}^{N} \omega_2(\mathbf{x}_j)(\cos\phi I_{xj} + \sin\phi I_{yj}) \quad \text{during pulse of phase } \phi, \qquad [27]$$

where $\mathbf{x}_j$ is the spatial coordinate of the jth spin. Evaluating the zeroth-order Magnus expansion term for $\tilde{\mathcal{H}}_\epsilon(t)$, integrating over both pulses and windows in the toggling frame, we find

$$\bar{\mathcal{H}}_\epsilon^{(0)} = 0. \qquad [28]$$

EMSL-30 is fundamentally different from most previous multiple-pulse sequences in a number of respects: the windows in EMSL-30 are a determinate length; EMSL-30 contains no solid echo pulse groups; EMSL-30 utilizes both 90° and 180° pulses; and the effective resonance offset precession axis is parallel to the rotating-frame z-axis and does not deviate from this direction as the offset frequency is varied, provided that $\omega_1 \gg \delta$.

The free evolution periods in EMSL-30 can be altered or inserted before the first pulse without changing the zeroth-order effective Hamiltonians displayed in Eqs. [25], [26], and [28], provided that the sum of all free evolution periods equals $6t_p$. Simulated and experimental tests indicate some variation in decoupling effectiveness as the durations of free evolution periods are adjusted. A key factor in optimizing the performance of the sequence is to ensure that $\bar{\mathcal{H}}_d^{(0)}$ is zero when integrating both to the midpoint and to the end of the sequence. Development of the earliest multiple-pulse decoupling sequences was guided by the realization that long, highly refined decoupling sequences could be constructed by concatenating shorter subunits that themselves had $\bar{\mathcal{H}}_d \approx 0$ (*1, 2, 7, 14, 15, 28, 29, 32*), which ensures that homonuclear dipolar evolution is suppressed over both short and long timescales during the whole sequence. By analogy with this past work, versions of EMSL-30 composed of subunits that periodically suppress the homonuclear dipolar evolution within the sequence may be expected to be more effective than variants with $\bar{\mathcal{H}}_d^{(0)} = 0$ only at the end of the sequence.

Windowless and semiwindowless homonuclear decoupling sequences have been proposed by Burum *et al.* (*37*), Liu *et al.* (*38*), and Hafner and Spiess (*39*). Unlike the windowless

sequences, EMSL-30 contains gaps that permit sampling of the entire multiple-pulse transient in one scan. EMSL-30 is also distinguished from these past sequences by the z-direction of its precession axis.

Hohwy and co-workers, who independently realized the desirability of decoupling sequences with an effective precession axis parallel to the z-direction, have recently proposed longer sequences with characteristics similar to those of EMSL-30 (*40, 41*). Initial results reported by them indicate that the decoupling performance of their sequences is comparable to the best of previous sequences, and is superior in certain respects, such as decoupling uniformity over a range of offsets. Their promising findings are consistent with the analysis presented here, which implies that the advantages of having the precession axis collinear with z include other factors besides artifact suppression and broader bandwidths.

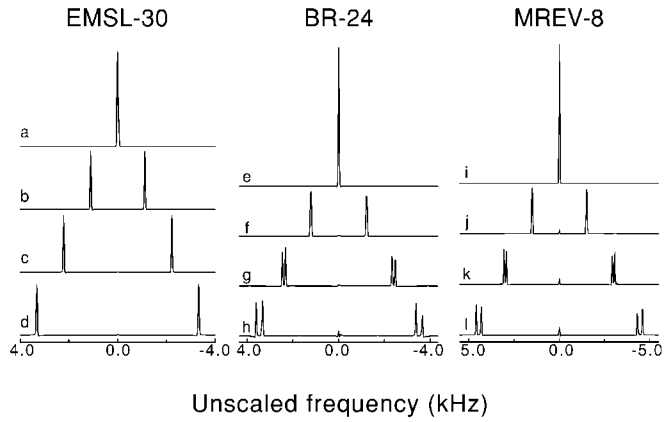

FIG. 5. Simulated EMSL-30, BR-24, and MREV-8 spectra of an isolated two-proton spin system with $\delta_1 = -\delta_2$. Values of δ_1 are 0.0 kHz (a, e, i), 3.0 kHz (b, f, j), 6.0 kHz (c, g, k), and 9.0 kHz (d, h, l). The EMSL-30 and MREV-8 spectral, widths have been truncated to the middle 8.0- and 11.0-kHz sections, respectively, while the entire BR-24 spectral width is displayed.

SIMULATIONS

Methods and Parameters

The simulated multiple-pulse NMR transients we report here were computed by numerically integrating the equations of motion of the density matrix (*42, 43*). The programs we have written to perform these calculations incorporate C++ objects contained in the mathematical shell of the GAMMA library created by Smith *et al.* (*44*). In every simulation shown below, the Hamiltonian during rf pulses includes the dipolar and resonance offset interactions in addition to $\mathcal{H}_{rf}$.

In most multiple-pulse experiments, the sampling window and 90° pulse width cannot be shortened below certain minimum values. We have assumed that these minimum values are 4.8 μs for the sampling window, and 1.6 μs for the 90° pulse width, for all simulations. Given these values, the MREV-8 and BR-24 τ value, as corrected for finite pulse widths (*2, 35*), is 3.2 μs, giving us MREV-8 and BR-24 cycle times of 38.4 and 115.2 μs, respectively. For EMSL-30, the 1.6-μs 90° pulse width implies a cycle time of 48.0 μs. In all cases, the data are acquired at the end of the last window of the cycle.

Each EMSL-30 spectrum was obtained from two interferograms, the first computed with a prepulse phase of 90° and a receiver phase of 0°, and the second computed with a prepulse phase of 270° and a receiver phase of 180°, and the results were added. The flip angle of the prepulse was $\pi/2$ in both cases. The simulated BR-24 spectra are products of a two-step phase cycle (*6*) that minimizes the DC and image frequency artifacts caused by the tilted axis precession of the magnetization. Similarly, the MREV-8 spectra are products of a four-step phase cycle. The versions of BR-24 and MREV-8 programmed in these simulations are shown in Table 1.

The range of frequencies that are contained in spectra obtained with these sequences can be estimated from the offset scaling factors given in Table 1 and Eq. [26]. For the cycle times specified above, the scaled spectral widths in zeroth order are 55.24 kHz (MREV-8), 22.55 kHz (BR-24), and 56.31 kHz (EMSL-30).

Two Protons with $\delta_1 = -\delta_2$

Figure 5 shows simulated spectra of a two-proton, single-orientation spin system for EMSL-30, BR-24, and MREV-8. The carrier frequency has been positioned so $\delta_1 = -\delta_2$. The interproton distance is 2.03 Å and the magnetic field is perpendicular to the interproton vector in these calculations. These simulations reveal that the performance of EMSL-30 is superior to that of BR-24 and MREV-8 in several respects. The first is in its greater effectiveness in suppressing the dipolar splitting of the two chemical shift resonances at nonzero offsets. While a residual dipolar splitting is clearly observable in the MREV-8 and BR-24 spectra for $\delta_1 = -\delta_2 = 6.0$ kHz, the EMSL-30 spectra show no reduction in line-narrowing effectiveness at resonance offsets 50% larger. A second feature to observe is that the zero-frequency spin-lock "pedestal" and other spectral artifacts are less prominent in the EMSL-30 spectra, despite the use of a phase-cycling scheme in the calculation of the BR-24 and MREV-8 interferograms (*6*).

For all three sequences, associated with an increase in the offset difference $2\delta_1$ is the formation of a splitting in the resonances of the two protons. This splitting is the manifestation of the incomplete suppression of the two-proton dipolar interaction and the growth of $\bar{\mathcal{H}}_d$ as the offsets increase. In the case of MREV-8, the growth of $\bar{\mathcal{H}}_d$ is indicated, in zeroth order, by the antidiagonal of Fig. 3d.

EMSL-30 has two additional advantages over BR-24 and MREV-8 that are not visible in these or the succeeding simulated spectra. The first is that 100% of the spin magnetization contributes to the spectral intensity of an EMSL-30 experiment, while about 68 and 60% of the magnetization is preserved in BR-24 and MREV-8 experiments, respectively, after

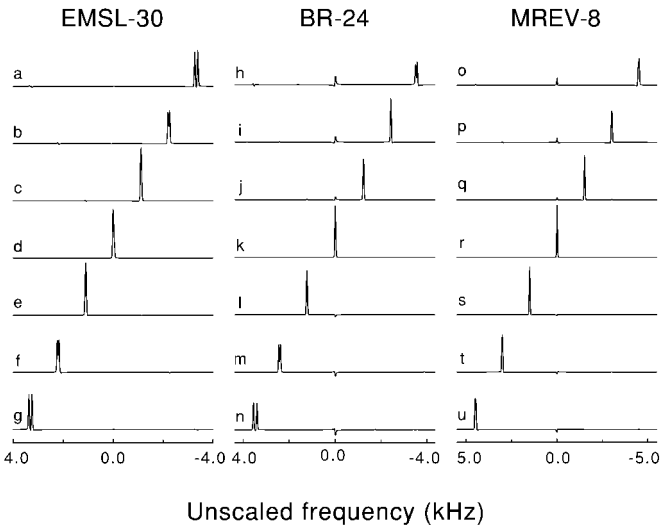

FIG. 6. Simulated EMSL-30, BR-24, and MREV-8 spectra of an isolated proton pair spin system with $\delta_1 = \delta_2$. Resonance offsets are −9.0 kHz (a, h, o); −6.0 kHz (b, i, p); −3.0 kHz (c, j, q); 0.0 kHz (d, k, r); 3.0 kHz (e, l, s); 6.0 kHz (f, m, t); and 9.0 kHz (g, n, u).

phase cycling. There is a loss in signal intensity for the latter two experiments because a fraction of the signal in single-scan BR-24 and MREV-8 spectra is contained in undesired artifact lines (*6*). These artifact signals are canceled by the phase cycling, but this procedure results in a partial subtraction of signal intensity. The second unseen advantage of the EMSL-30 sequence is that it has a larger effective bandwidth than the other two sequences. While the cycle time of MREV-8 is shorter in these simulations, the range of offsets that can be contained in an EMSL-30 spectrum is slightly larger than that for MREV-8 due to the smaller offset scaling factor of EMSL-30. Without the use of phase cycles, the effective spectral width of the BR-24 and MREV-8 experiments is halved, and the advantage of EMSL-30 would be even greater.

Two Protons with $\delta_1 = \delta_2$

Simulated spectra of two dipolar-coupled protons with identical resonance offsets are shown in Fig. 6. Besides the resonance offsets, all other parameters are the same as those for Fig. 5. The decoupling of the two protons by EMSL-30 in the range $-3.0 \leq \delta_1 \leq 3.0$ kHz is essentially complete. Spectral artifacts cannot be seen without substantial vertical expansion of the baseline, even for the larger offsets. The major distortion to appear at higher values of δ_1 is the formation of a residual dipolar splitting.

The dipolar splitting is suppressed for a slightly wider range of frequencies by BR-24. Although the line does not divide over this range, the intensity of the unsplit line decreases visibly, even for offsets within ±3.0 kHz. Also, the zero-frequency artifact can be clearly seen in every off-resonance spectrum.

MREV-8 is the most effective in suppressing the residual splitting of the three sequences. This is partly explained by observing that MREV-8 has the shortest cycle time, and so these simulations actually almost satisfy the coherent averaging assumption $T^{-1} \gg \delta$ over the entire offset range. The relative magnitude of $\bar{\mathcal{H}}_d$ in the offset-toggled frame may be estimated, in zeroth order, by considering the diagonal of Fig. 3d. This figure reveals that within the range of offsets shown in Fig. 6, $\bar{\mathcal{H}}_d$ is scaled to less than 10% of its undecoupled value, and thus does not produce a splitting that can be resolved in the simulation.

Two Protons with $\delta_1 = 0$, $\delta_2 \neq 0$

We conclude from Fig. 6 that in the absence of pulse imperfections and chemical shift differences of coupled spins, the carrier frequency should be tuned exactly on resonance with the NMR lines for optimum decoupling. In Fig. 7 we examine the performance of these sequences if the two coupled spins have different resonance frequencies and one spin is on resonance.

For all three sequences, obvious spectral distortions appear as early as $\delta_2 = \pm 3.0$ kHz. The off-resonance line is the most distorted in the EMSL-30 and BR-24 spectra, but for MREV-8 the on-resonance line has a larger residual splitting than the off-resonance transition.

These results suggest that the resolution of a single resonance in a multiline spectrum may not always be improved by tuning the spectrometer frequency to the desired line if the resonant spin is strongly coupled to spins that are far off resonance. In cases where strong couplings between spins with

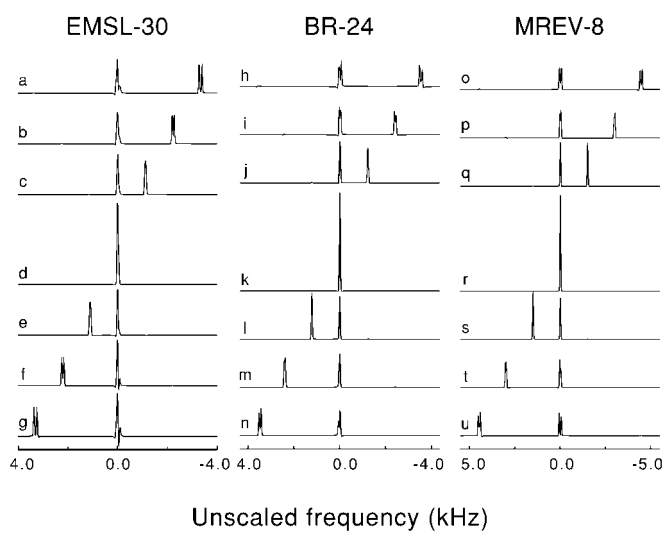

FIG. 7. Simulated EMSL-30, BR-24, and MREV-8 spectra of an isolated two-proton spin system. One proton is exactly on resonance, and the resonance offset of the second proton is 9.0 kHz (a, h, o); 6.0 kHz (b, i, p); 3.0 kHz (c, j, q); 0.0 kHz (d, k, r); −3.0 kHz (e, l, s); −6.0 kHz (f, m, t); and −9.0 kHz (g, n, u).

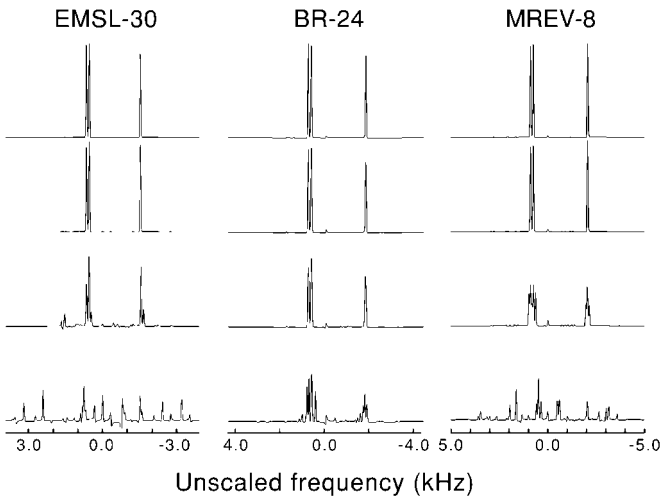

FIG. 8. Simulated EMSL-30, BR-24, and MREV-8 spectra of an isolated three-proton spin system. The protons form an equilateral triangle, with an interproton distance of 3.23 Å (a, e, i); 2.56 Å (b, f, j); 2.03 Å (c, g, k); and 1.61 Å (d, h, l).

large chemical shift differences exist, the optimal position for the carrier frequency may be at some intermediate frequency.

Three Protons

The effects of higher order spin correlations on decoupling performance are considered in three-proton simulations represented by the spectra in Fig. 8. These simulations also reveal the distortions that develop in multiple-phase spectra as the homonuclear dipolar coupling increases. In these calculations, the three protons are assumed to be positioned at the vertices of an equilateral triangle, with the magnetic field pointing orthogonally to the plane defined by the three protons. The protons are magnetically inequivalent, with resonance offsets of 1.8, 1.5, and -4.1 kHz. The values of the dipolar couplings increase in the ratio of 1:2:4:8 going from spectra (a) to (d). The pulse sequence parameters and phase cycle are the same as those for Fig. 5.

All three sequences are effective in suppressing the homonuclear dipolar interaction for internuclear distances down to 2.56 Å. The zero-frequency artifact is seen in the MREV-8 and BR-24 spectra, even for couplings and offsets that are small compared to the inverse cycle time. With slight expansion of the vertical scale, mirror image artifacts also become visible in the BR-24 and MREV-8 spectra.

As the internuclear distance is decreased to 2.03 Å and below, there is a rapid degradation in line-narrowing performance of both MREV-8 and EMSL-30. BR-24 performs better in the strong coupling simulations, but the resolution is affected, too, by the decrease in interproton distance from 2.56 to 2.03 Å.

All of the two-proton simulations shown in Figs. 5–7 were computed assuming an internuclear distance of 2.03 Å. Unlike the three-proton simulations, for $r_{H-H} = 2.03$ Å and below, all three sequences appeared to be effective in suppressing the two-spin homonuclear dipolar evolution for a range of offsets. This finding reveals the significant influence N-spin correlations, $N > 2$, may have in determining the resolution of multiple-pulse spectra for spin systems with more than two strongly coupled spins, and suggests that relatively small changes in the geometry of the proton network can result in major differences in decoupling performance. Past investigations on two-spin systems, such as experiments on gypsum single crystals (*45*), provide some evidence that strong dipolar interactions may in fact be more readily eliminated by multiple-pulse sequences when the spins are coupled in pairs rather than in larger networks.

EXPERIMENTS

Methods and Parameters

Experimental results were obtained on a Chemagnetics CMX Infinity console, operating at a proton Larmor frequency of 299.99 MHz. A Chemagnetics CRAMPS probe was used for all experiments. The rf pulse times and phases were tuned and calibrated according to standard procedures (*46–48*) on the proton resonance of poly(dimethylsiloxane) (P(DMS)). The 90° pulse width was 1.6 μs, and the MREV-8 and BR-24 cycle times were 48.0 and 144.0 μs, respectively, with short and long window lengths adjusted for finite pulse widths as reported by Mehring (*35*). Data for the MREV-8 and BR-24 experiments were acquired at the ends of the long windows, immediately before the first pulse of the next cycle. The versions of BR-24 and MREV-8 implemented in these experiments are specified in Table 1. Four- and eight-step phase cycles were employed in the BR-24 and MREV-8 experiments, respectively, to suppress artifacts caused by the tilted axis precession of the magnetization (*6*). A four-step phase cycle of the prepulse and receiver phases was used in the EMSL-30 experiments.

Levitt and co-workers (*49–51*) and Waugh (*18*) have previously described ways to improve the performance of cyclic heteronuclear liquid-state decoupling sequences. These methods consist of iterative rules for grouping modified versions of a decoupling sequence to form longer sequences called supercycles. Most of the specific rules they developed cannot be adapted for homonuclear decoupling sequences such as MREV-8 or BR-24, but some of the ideas can be applied to EMSL-30. For example, error terms in the effective dipolar and shift Hamiltonians of EMSL-30 with the transformation property

$$R_z(\pi)\bar{\mathcal{H}}_\epsilon R_z^{-1}(\pi) = -\bar{\mathcal{H}}_\epsilon \qquad [29]$$

can be eliminated to zeroth order by concatenating EMSL-30 with a version of itself modified by a shift of the phases of all pulses of 180°. Similarly, error terms obeying the equality

$$R_z(\pi/2)\bar{\mathcal{H}}_\epsilon R_z^{-1}(\pi/2) = -\bar{\mathcal{H}}_\epsilon \quad [30]$$

are eliminated to zeroth order by concatenating EMSL-30 with a version of itself modified by a shift of the phases of all pulses by 90°. A zeroth-order analysis of the EMSL-30 error terms would suggest, therefore, that the supercycle $P_0P_\pi P_{\pi/2}P_{3\pi/2}$, where P_ϕ denotes an EMSL-30 sequence with all pulse phases shifted by ϕ radians, would achieve a decoupling performance that was superior to a single EMSL-30 cycle. We have indeed found that the spectra are significantly improved by substituting the EMSL-30 supercycle (which we denote EMSL-30s) for EMSL-30. In this paper, we show only EMSL-30s experimental results. Despite the longer cycle time of EMSL-30s, the interferogram was acquired at the rate of one point per EMSL-30 cycle, or four points per EMSL-30s cycle, thus preserving the bandwidth of the original EMSL-30 sequence.

Frequency Offset Measurements

The scaling of NMR frequency offsets by multiple-phase sequences was experimentally determined by measuring the position of the proton resonance of P(DMS) relative to the spectrum center as a function of the spectrometer carrier frequency. We have compared the predictions of the zeroth-order coherent averaging theory with experimental results for MREV-8 and BR-24 (Fig. 9) by plotting the *deviation* of the measurements from the zeroth-order theoretical values, as evaluated with

$$\Delta = (\delta^{(\mathrm{obs})} - S^{(0)}\delta)T, \quad [31]$$

where $\delta^{(\mathrm{obs})}$ is the measured offset, $S^{(0)}$ is the zeroth-order coherent averaging theory scale factor, and δ is defined by $\omega_{\mathrm{P(DMS)}} - \omega_{\mathrm{rf}}$. The zeroth-order scaling factors for MREV-8 and BR-24 were calculated using the equations of Burum *et al.* (*37*), which include a correction for finite pulse widths.

The discrepancy between the experimental results and the zeroth-order theoretical predictions is systematic, and cannot be explained by experimental error or an incorrect choice of the scale factor. Pulse imperfections, which were quantified during the tuning procedure, are not of sufficient size to account for the discrepancy. The nonlinearity of the measured frequency offset is particularly significant at the extrema of the spectrum, where the zeroth-order approximation $T^{-1} \gg \delta$ does not hold. As shown by the solid curves in Fig. 9, the nonlinear offsets calculated using the exact theory correlate well with the experimentally measured offsets over the entire Nyquist bandwidth of the multiple-phase spectrum, even near the ends of the spectrum where nonlinear effects are greatest. The agreement between theory and experiment is further improved as the duty cycle and the 90° pulse width are decreased.

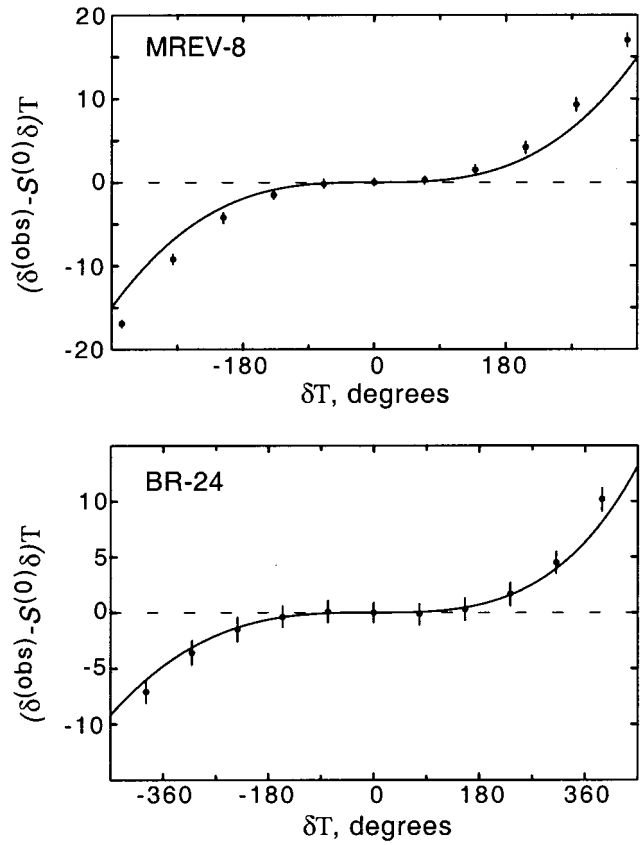

FIG. 9. Deviation from linearity of the frequency shifts observed in MREV-8 (top) and BR-24 (bottom) experiments as a function of δT. Filled circles are experimental data and bars are full-width half-height linewidths. Solid curves are the deviations calculated using the exact theory.

Solid-State Proton Spectra

Figure 10 shows EMSL-30s, BR-24, and MREV-8 proton spectra of a dimethylnaphthalene single crystal measured at three different carrier frequencies. The same number of scans was acquired for each spectrum.

The resolution of the EMSL-30s and BR-24 spectra is comparable, and the resolution of the MREV-8 spectra is the worst of the three. The BR-24 and MREV-8 spectra in all cases contain a pronounced zero-frequency spike indicative of the incomplete cancellation of the "pedestal" signal by the phase cycle (*6*). This artifact is absent in the EMSL-30s spectrum.

An important advantage of multiple-pulse sequences like EMSL-30s having $\bar{\mathcal{H}}_\delta^{(0)} \propto \mathcal{H}_\delta$ is demonstrated by the intensities of the EMSL-30s spectra compared to the intensities of the other two sequences. Although each spectrum represents the same number of scans, the EMSL-30s spectra clearly contain more signal than the BR-24 and MREV-8 spectra. As discussed above and elsewhere (*6*), significant amounts of signal intensity in MREV-8 and BR-24 spectra are lost in the form of unavoidable spectral artifacts. EMSL-30s is not afflicted by these artifacts, and thus EMSL-30s spectra contain considerably more useful signal than MREV-8 and BR-24 spectra.

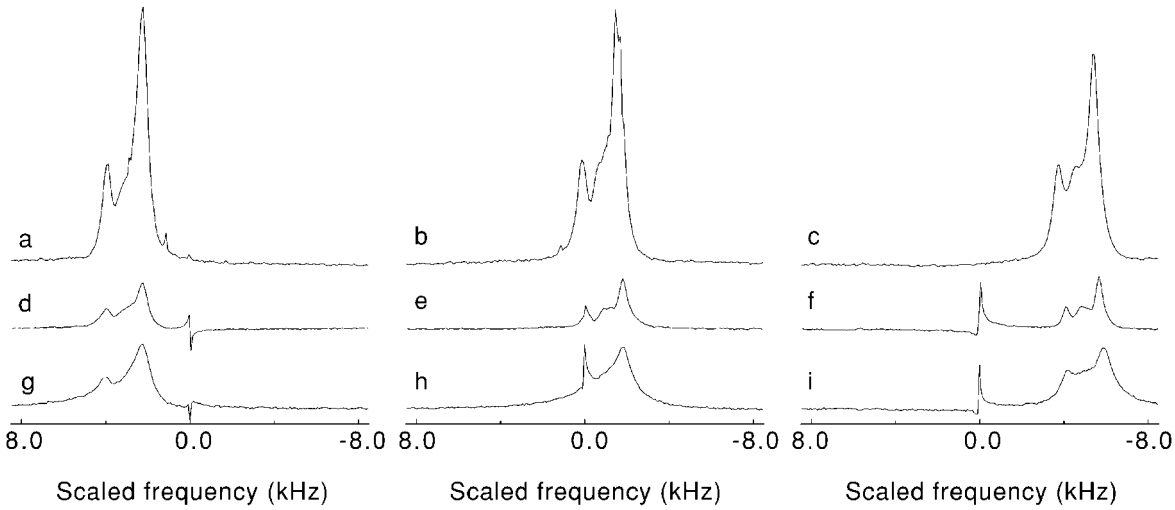

FIG. 10. Mutiple-pulse proton spectra of a dimethylnaphthalene single crystal. The carrier frequency increases in 4-kHz increments from left to right. The decoupling sequences were EMSL-30s (a, b, c), BR-24 (d, e, f), and MREV-8 (g, h, i). The position of the carrier frequency in each spectrum is at 0.0 kHz.

Figure 10 shows only a fraction of the total spectral widths acquired in these spectra. Based on the zeroth-order scaling factors, the range of offsets that can be observed in the experimental spectra can be estimated to be 56.3 kHz (EMSL-30s), 18.0 kHz (BR-24), and 44.2 kHz (MREV-8). For higher field measurements or nuclei with larger chemical shift ranges, such as ^{19}F, the increased spectral width will be an attractive feature of the EMSL-30s experiment.

The results displayed in Fig. 11 confirm that EMSL-30s works equally well in CRAMPS applications (*52*, *53*). Each spectrum in this figure is the sum of an equal number of scans. While the EMSL-30s lines appear to be wider at the base than BR-24 resonances, the half-height linewidths are less.

CONCLUSION

The critical first step in a coherent averaging theory analysis of multiple-pulse dynamics is the choice of an interaction representation. In making this decision, the main task is to differentiate between interactions that have a large, easily analyzed effect on the spin system's dynamics and those that have a small, perturbative effect.

Low-order coherent averaging theory approximations are accurate when the terms in the perturbation Hamiltonian V are small in both the original frame *and* the interaction frame. The discrepancy we have discovered between coherent averaging theory results and exact calculations arises because the reso-

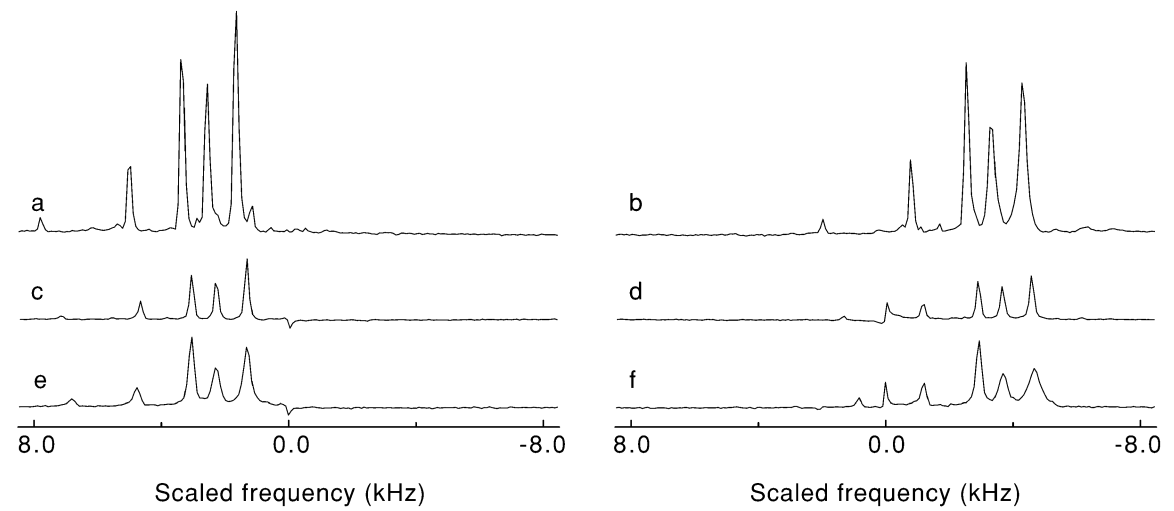

FIG. 11. Proton CRAMPS spectra of fumaric acid monoethyl ester powder acquired with 1 kHz sample spinning. The carrier frequencies increase by 6 kHz from left to right. The decoupling sequences were EMSL-30s (a, b), BR-24 (c, d), and MREV-8 (e, f). The position of the carrier frequency in each spectrum is at 0.0 kHz.

nance offset is a small interaction in the rotating frame but a large interaction in the toggling frame (compared to T^{-1}) if $\mathcal{H}_\delta$ is included in part of V. In cases where it is found that $\bar{V}$ is not small relative to T^{-1}, one must question the validity of approximating $\bar{V}$ with only low-order terms, or else reevaluate the specification of the interaction representation.

In this paper, the latter approach is followed. We have determined from this treatment that spectra obtained by multiple-pulse homonuclear decoupling methods become significantly distorted when the spectrometer carrier frequency is off resonance, even if the spectrometer's performance is otherwise ideal. The magnitude of many of these distortions, including residual dipolar line broadening, nonlinearity of offset frequency scaling, and tilted axis precession artifacts, can be quantified in the offset-toggled frame over the entire Nyquist bandwidth, which is not readily accomplished in the traditional toggling frame.

In investigating the off-resonance dynamics of nuclear spins during multiple-pulse irradiation, simulations can be an important aid. In experimental studies, many difficult-to-quantify factors affect the observed outcome, including pulse imperfections, nonideal instrument performance, and relaxation effects. Furthermore, it is usually not feasible to vary systematically certain parameters, e.g., chemical shifts and spin–spin couplings, associated with the sample in order to elucidate the influence of these quantities on dynamics. The combination of these factors interferes with attempts to isolate the effect of a single interaction, such as the resonance offset. Time-domain simulations are an appealing alternative for such investigations.

NMR spectrometer design has been a prime focus of efforts to improve the performance of multiple-pulse experiments. Unless the spectrometer, probe, and transmitter are well designed and tuned, instrumental deficiencies will indeed severely limit the resolution that can be observed in a solid-state homonuclear decoupling experiment. As calculations in the offset-toggled frame, exemplified by Fig. 3, indicate though, spectrometer performance will not be the ultimate resolution-limiting factor for dispersed spectra obtained with WAHUHA, MREV-8, BR-24, or related sequences. On a well-tuned NMR spectrometer, further improvements in off-resonance decoupling results will only be achieved by utilizing sequences such as EMSL-30 based on different design principles.

EMSL-30 is superior to previously described sequences in other respects, including bandwidth, sensitivity, and freedom from tilted axis precession artifacts. Multiple-phase decoupling sequences having an effective precession axis parallel to the rotating-frame z-axis will also be preferable in 2D experiments, such as heteronuclear correlation measurements (*54–57*), homonuclear dipolar shift correlation experiments (*58*), and solid-state COSY methods (*43, 59*). On the other hand, BR-24, which is designed to be self-compensated for pulse sequence imperfections, seems to achieve better line narrowing when spectrometer performance is deficient, especially near resonance. For multiple-pulse spectra with all of the lines contained in a chemical shift range that is narrow relative to the Nyquist bandwidth, the resolution of on-resonance BR-24 spectra is still as good or better than EMSL-30 spectra obtained with current spectrometer technology.

The off-resonance effects reported in this paper will become increasingly prominent in future NMR experiments performed at higher fields on improving instrumentation. Gains in resolution and sensitivity will not be commensurate unless new sequences with better off-resonance characteristics are devised.

Coherent averaging theory and the concept of effective Hamiltonians have influenced the analysis and formulation of time-domain magnetic resonance experiments beyond the original applications in homonuclear decoupling sequences in solids. Some examples include multiple-quantum NMR experiments (*60*), solution-state heteronuclear decoupling sequences (*18, 49–51, 61*), numerous multidimensional NMR mixing schemes (*43*), zero-field NMR in high field (*48*), and rf-driven electron spin echo envelope modulation (ESEEM) spectroscopy (*62*). As is the case in decoupling experiments with the chemical shift Hamiltonian, the goal in many of these experiments is to specify and maximize an effective Hamiltonian that is different from the rotating-frame Hamiltonian. It has been demonstrated here that there is potentially an inconsistency in calculating large, nonzero effective Hamiltonians with low-order approximations, except for the shortest cycle times. A combination of exact calculations, numerical simulations, and evaluation of higher order terms is essential in these situations for determining if the deviation from the desired effective Hamiltonian is significant and affects experimental observations.

APPENDIX A

In this appendix, we prove two propositions about the rotation matrix $R_{\mathbf{r}}(\psi)$ given in Eq. [8]: (a) ψ and β are independent of the values of τ_b and τ_e, provided that the sum $\tau_b + \tau_e$ is held fixed; and (b) S and β are invariant with respect to a change in the sign of δ.

To prove (a), we consider two rotation operators of the form given by Eq. [8]:

$$R_{\mathbf{r}_1}(\psi_1) = R_z(\delta\tau_{e,1})\,R_{\bar{x}}(\pi/2)\,R_z(\delta\tau_s)\,R_y(\pi/2)\,R_z(\delta\tau_l) \times R_{\bar{y}}(\pi/2)\,R_z(\delta\tau_s)\,R_x(\pi/2)\,R_z(\delta\tau_{b,1}), \quad [A1]$$

$$R_{\mathbf{r}_2}(\psi_2) = R_z(\delta\tau_{e,2})\,R_{\bar{x}}(\pi/2)\,R_z(\delta\tau_s)\,R_y(\pi/2)\,R_z(\delta\tau_l) \times R_{\bar{y}}(\pi/2)\,R_z(\delta\tau_s)\,R_x(\pi/2)\,R_z(\delta\tau_{b,2}), \quad [A2]$$

with

$$\tau_{e,1} + \tau_{b,1} = \tau_{e,2} + \tau_{b,2}. \quad [A3]$$

From Eq. [A3], we can write $\tau_{b,1} = \tau_{b,2} + \tau_\Delta$ and $\tau_{e,1} = \tau_{e,2} - \tau_\Delta$, and

$$R_{\mathbf{r}_1}(\psi_1) = R_z(\delta\tau_\Delta)\, R_{\mathbf{r}_2}(\psi_2)\, R_z^{-1}(\delta\tau_\Delta). \qquad \text{[A4]}$$

Waugh (*18*) has shown that from the matrix form of $R_{\mathbf{r}_1}(\psi_1)$ in the irreducible representation of the rotation group $SU(2)$ (*63*), one can compute ψ_1 via the relationship

$$\psi_1 = 2\,\cos^{-1}(\zeta_1/2), \qquad \text{[A5]}$$

where ζ_1 is the trace of $R_{\mathbf{r}_1}(\psi_1)$. Since, by Eq. [A4], $R_{\mathbf{r}_1}(\psi_1)$ and $R_{\mathbf{r}_2}(\psi_2)$ are related by a similarity transformation, their traces must be equal, and $\psi_1 = \psi_2$ by Eq. [A5]. A similar argument can be constructed to show $\beta_1 = \beta_2$. By hypothesis, $\tau_{e,1}$, $\tau_{b,1}$, $\tau_{e,2}$, and $\tau_{b,2}$ can have any values, subject to the constraint represented by Eq. [A3]. Thus, Proposition (a) is proved: ψ and β are independent of the values of τ_b and τ_e, provided that the sum $\tau_b + \tau_e$ is held fixed. From Eq. [12], we infer that the same statement applies to S.

The equalities $\psi_1 = \psi_2$ and $\beta_1 = \beta_2$ both derive from a more fundamental property of rotation operators,

$$R_{\mathbf{r}_\chi}(\chi)\, R_{\mathbf{r}}(\psi)\, R_{\mathbf{r}_\chi}^{-1}(\chi) = R_{\mathbf{r}'}(\psi), \qquad \text{[A6]}$$

with $\mathbf{r}' = R_{\mathbf{r}_\chi}(\chi)\mathbf{r}$.

Proposition (b) follows directly from (a). The quantities S and β are invariant with respect to a change in the sign of δ for at least one combination of τ_b and τ_e values, *viz.*, $\tau_b = \tau_e$. We have discussed earlier how this invariance derives from the symmetry of the WAHUHA toggling-frame Hamiltonian, $\tilde{\mathcal{H}}_\delta(t)$, and seen in Fig. 2 the confirmation that β and S are even functions of δT. If β and S are even functions of δT for one pair (τ_b, τ_e) values, however, then they must be even functions of δT for all pairs of (τ_b, τ_e) values, provided that $\tau_b + \tau_e$ is fixed, since all curves for fixed $\tau_b + \tau_e$ must coincide by Proposition (a). This proves Proposition (b).

As exemplified by Eq. [14], odd-order terms in the Magnus expansion of the WAHUHA toggling-frame Hamiltonian $\mathcal{H}_\delta(t)$ are not zero when $\tau_b \neq \tau_e$. Based on this observation, one might expect that β and S could not be even functions of δT unless $\tau_b = \tau_e$. It is interesting to observe, therefore, that this expectation is incorrect. We conclude that while individual odd-order terms of this operator expansion are not zero, the sum of the odd-order terms must converge to zero for all δ. Unlike a Fourier or Chebyshev series, the convergence of the sum of odd-order Magnus expansion terms to zero is possible because: (1) the function that is being expanded does not commute with itself at different times; and (2) each term in the expansion is not orthogonal to all of the other terms.

APPENDIX B

$\bar{\mathcal{H}}^{(0)}_{d,1}$, $\bar{\mathcal{H}}^{(0)}_{d,2}$, and $\bar{\mathcal{H}}^{(0)}_{d,3}$ in Eq. [22] can be calculated by straightforward applications of known formulas (*2*). The results are

$$\begin{aligned}\bar{\mathcal{H}}^{(0)}_{d,1} = \frac{1}{2}\sum_{\substack{j,k=1\\ j\neq k}}^{N} d_{jk}\{&2I_{zj}I_{zk} - \mathrm{sinc}(\xi_{j1}-\xi_{k1})(I_{xj}I_{xk}+I_{yj}I_{yk})\\ &+ (\xi_{j1}-\xi_{k1})^{-1}[\cos(\xi_{j1}-\xi_{k1})-1]\\ &\times (I_{xj}I_{yk}-I_{yj}I_{xk})\}, \qquad \text{[B1]}\end{aligned}$$

$$\begin{aligned}\bar{\mathcal{H}}^{(0)}_{d,2} = \frac{1}{2}\sum_{\substack{j,k=1\\ j\neq k}}^{N} d_{jk}\{&-I_{zj}I_{zk}\mathrm{sinc}(\xi_{j2}-\xi_{k2})\\ &+ I_{xj}I_{xk}[2\sin\xi_{j1}\sin\xi_{k1} - \mathrm{sinc}(\xi_{j2}-\xi_{k2})\\ &\times\cos\xi_{j1}\cos\xi_{k1}] + I_{yj}I_{yk}[2\cos\xi_{j1}\cos\xi_{k1}\\ &- \mathrm{sinc}(\xi_{j2}-\xi_{k2})\sin\xi_{j1}\sin\xi_{k1}]\\ &+ I_{xj}I_{yk}[2\sin\xi_{j1}\cos\xi_{k1} + \mathrm{sinc}(\xi_{j2}-\xi_{k2})\\ &\times\cos\xi_{j1}\sin\xi_{k1}] + I_{yj}I_{xk}[2\cos\xi_{j1}\sin\xi_{k1}\\ &+ \mathrm{sinc}(\xi_{j2}-\xi_{k2})\sin\xi_{j1}\cos\xi_{k1}] + (\xi_{j2}-\xi_{k2})^{-1}\\ &\times[\cos(\xi_{j2}-\xi_{k2})-1](I_{zj}I_{xk}\cos\xi_{k1}\\ &- I_{zj}I_{yk}\sin\xi_{k1} - I_{xj}I_{zk}\cos\xi_{j1} + I_{yj}I_{zk}\sin\xi_{j1})\}, \qquad \text{[B2]}\end{aligned}$$

$$\begin{aligned}\bar{\mathcal{H}}^{(0)}_{d,3} = \frac{1}{2}\sum_{\substack{j,k=1\\ j\neq k}}^{N} d_{jk}\{&(I_{xj}I_{xk}\cos\xi_{j1}\cos\xi_{k1} - I_{xj}I_{yk}\cos\xi_{j1}\sin\xi_{k1}\\ &- I_{yj}I_{xk}\sin\xi_{j1}\cos\xi_{k1} + I_{yj}I_{yk}\sin\xi_{j1}\sin\xi_{k1})\\ &\times[2\cos\xi_{j2}\cos\xi_{k2} - \mathrm{sinc}(\xi_{j3}-\xi_{k3})\sin\xi_{j2}\sin\xi_{k2}]\\ &+ (I_{xj}\cos\xi_{j1} - I_{yj}\sin\xi_{j1})I_{zk}[2\cos\xi_{j2}\sin\xi_{k2}\\ &+ \mathrm{sinc}(\xi_{j3}-\xi_{k3})\sin\xi_{j2}\cos\xi_{k2}]\\ &+ (I_{xk}\cos\xi_{k1} - I_{yk}\sin\xi_{k1})I_{zj}[2\sin\xi_{j2}\cos\xi_{k2}\\ &+ \mathrm{sinc}(\xi_{j3}-\xi_{k3})\cos\xi_{j2}\sin\xi_{k2}]\\ &+ I_{zj}I_{zk}[2\sin\xi_{j2}\sin\xi_{k2} - \mathrm{sinc}(\xi_{j3}-\xi_{k3})\\ &\times\cos\xi_{j2}\cos\xi_{k2}] - \mathrm{sinc}(\xi_{j3}-\xi_{k3})\\ &\times[I_{yj}I_{yk}\cos\xi_{j1}\cos\xi_{k1} + I_{xj}I_{yk}\sin\xi_{j1}\cos\xi_{k1}\\ &+ I_{yj}I_{xk}\cos\xi_{j1}\sin\xi_{k1} + I_{xj}I_{xk}\sin\xi_{j1}\sin\xi_{k1}]\\ &- (\xi_{j3}-\xi_{k3})^{-1}[\cos(\xi_{j3}-\xi_{k3})-1]\\ &\times[I_{zk}\cos\xi_{k2}(I_{yj}\cos\xi_{j1} + I_{xj}\sin\xi_{j1})\\ &- I_{zj}\cos\xi_{j2}(I_{yk}\cos\xi_{k1} + I_{xk}\sin\xi_{k1})\\ &- \sin\xi_{k2}(I_{yj}I_{xk}\cos\xi_{j1}\cos\xi_{k1} + I_{xj}I_{xk}\sin\xi_{j1}\cos\xi_{k1}\\ &- I_{yj}I_{yk}\cos\xi_{j1}\sin\xi_{k1} - I_{xj}I_{yk}\sin\xi_{j1}\sin\xi_{k1})\\ &+ \sin\xi_{j2}(I_{xj}I_{yk}\cos\xi_{j1}\cos\xi_{k1} + I_{xj}I_{xk}\cos\xi_{j1}\sin\xi_{k1}\\ &- I_{yj}I_{yk}\sin\xi_{j1}\cos\xi_{k1} - I_{yj}I_{xk}\sin\xi_{j1}\sin\xi_{k1})]\}, \qquad \text{[B3]}\end{aligned}$$

where $\xi_{jn} = \delta_j\tau_n$ and $\xi_{kn} = \delta_k\tau_n$, $n = 1, 2, 3$.

ACKNOWLEDGMENTS

The Pacific Northwest National Laboratory is operated for the U.S. Department of Energy by the Battelle Memorial Institute under Contract DE-AC06-76RLO-1830.

REFERENCES

1. U. Haeberlen and J. S. Waugh, Coherent averaging effects in magnetic resonance, *Phys. Rev.* **175,** 453 (1968).
2. U. Haeberlen, "High Resolution NMR in Solids: Selective Averaging," Academic Press, New York (1976).
3. F. J. Dyson, The radiation theories of Tomonaga, Schwinger, and Feynman, *Phys. Rev.* **75,** 486 (1949).
4. W. Magnus, On the exponential solution of differential equations for a linear operator, *Commun. Pure Appl. Math.* **7,** 649 (1954).
5. Throughout this paper, we will refer to the resonance offset as the nuclear spin resonance frequency minus the spectrometer carrier frequency. The resonance offset thus includes the chemical shift.
6. H. Cho, Tilted axis precession and phase-sensitive detection of nuclear magnetization, *J. Magn. Reson. A* **121,** 8 (1996).
7. M. Mehring, "Principles of High Resolution NMR in Solids," 2nd ed., Springer-Verlag, Berlin (1983).
8. W.-K. Rhim, D. D. Elleman, and R. W. Vaughan, Analysis of multiple-pulse NMR in solids, *J. Chem. Phys.* **59,** 3740 (1973).
9. W.-K. Rhim, D. P. Burum, and R. W. Vaughan, Extraction of quadrature phase information from multiple pulse NMR signals, *Rev. Sci. Instrum.* **47,** 720 (1976).
10. D. P. Burum, D. G. Cory, K. K. Gleason, D. Levy, and A. Bielecki, Quadrature detection of CRAMPS NMR data for maximum resolution and sensitivity, *J. Magn. Reson. A* **104,** 347 (1993).
11. T. M. Barbara and L. Baltusis, Phase-cycled, multiple-window-acquisition, multiple-pulse NMR spectroscopy, *J. Magn. Reson. A* **106,** 182 (1994).
12. U. Haeberlen, J. D. Ellett, Jr., and J. S. Waugh, Resonance offset effects in multiple-pulse NMR experiments, *J. Chem. Phys.* **55,** 53 (1971).
13. A. Pines and J. S. Waugh, Quantitative aspects of coherent averaging. Simple treatment of resonance offset processes in multiple-pulse NMR, *J. Magn. Reson.* **8,** 354 (1972).
14. D. P. Burum and W.-K. Rhim, Analysis of multiple pulse NMR in solids. III, *J. Chem. Phys.* **71,** 944 (1979).
15. A. N. Garroway, P. Mansfield, and D. C. Stalker, Limits to resolution in multiple-pulse NMR, *Phys. Rev. B* **11,** 121 (1975).
16. F. Bloch, Nuclear induction, *Phys. Rev.* **70,** 460 (1946).
17. R. P. Feynman, F. L. Vernon, and R. W. Hellwarth, Geometrical representation of the Schrödinger equation for solving Maser problems, *J. Appl. Phys.* **28,** 49 (1957).
18. J. S. Waugh, Theory of broadband spin decoupling, *J. Magn. Reson.* **50,** 30 (1982).
19. R. N. Bracewell, "The Fourier Transform and Its Applications," 2nd revised ed., McGraw–Hill, New York (1986).
20. J. S. Waugh, L. M. Huber, and U. Haeberlen, Approach to high-resolution NMR in solids, *Phys. Rev. Lett.* **20,** 180 (1968).
21. C. H. Wang and J. D. Ramshaw, Decay of multiple spin echoes in dipolar solids, *Phys. Rev. B* **6,** 3253 (1972).
22. P. Pechukas and J. C. Light, On the exponential form of time-displacement operators in quantum mechanics, *J. Chem. Phys.* **44,** 3897 (1966).
23. R. M. Wilcox, Exponential operators and parameter differentiation in quantum physics, *J. Math. Phys.* **8,** 962 (1967).
24. W. A. B. Evans, On some applications of the Magnus expansion in nuclear magnetic resonance, *Ann. Phys. (N.Y.)* **48,** 72 (1968).
25. D. P. Burum, Magnus expansion generator, *Phys. Rev. B* **24,** 3684 (1981).
26. M. M. Maricq, Application of average Hamiltonian theory to the NMR of solids, *Phys. Rev. B* **25,** 6622 (1982).
27. M. M. Maricq, Application of a folding transformation to the Magnus solution for the evolution of periodically time dependent systems, *J. Chem. Phys.* **85,** 5167 (1986).
28. P. Mansfield, Symmetrized pulse sequences in high resolution nmr in solids, *J. Phys. C* **4,** 1444 (1971).
29. P. Mansfield, M. J. Orchard, D. C. Stalker, and K. H. B. Richards, Symmetrized multipulse nuclear-magnetic resonance experiments in solids: Measurement of the chemical-shift shielding tensor in some compounds, *Phys. Rev. B* **7,** 90 (1973).
30. W.-K. Rhim, D. D. Elleman, and R. W. Vaughan, Enhanced resolution for solid state NMR, *J. Chem. Phys.* **58,** 1772 (1973).
31. W.-K. Rhim, D. D. Elleman, L. B. Schreiber, and R. W. Vaughan, Analysis of multiple pulse NMR in solids. II, *J. Chem. Phys.* **60,** 4595 (1974).
32. D. P. Burum and W.-K. Rhim, An improved NMR technique for homonuclear dipolar decoupling in solids. Application to polycrystalline ice, *J. Chem. Phys.* **70,** 3553 (1979).
33. D. G. Cory, A new multiple-pulse cycle for homonuclear dipolar decoupling, *J. Magn. Reson.* **94,** 526 (1991).
34. M. Mehring and J. S. Waugh, Magic-angle NMR experiments in solids, *Phys. Rev. B* **5,** 3459 (1972).
35. M. Mehring, Arbitrary pulse width in the four-pulse NMR experiment, *Z. Naturforsch. A* **27,** 1634 (1972).
36. H. Cho, A revised coherent averaging theory analysis of multiple pulse homonuclear decoupling sequences, Poster P102, *in* Abstracts of Posters, 38th Experimental NMR Conference, Orlando, Florida (1997).
37. D. P. Burum, M. Linder, and R. R. Ernst, Low-power multipulse line-narrowing in solid-state NMR, *J. Magn. Reson.* **44,** 173 (1981).
38. H. Liu, S. J. Glaser, and G. P. Drobny, Development and optimization of multipulse propagators: Applications to homonuclear decoupling in solids, *J. Chem. Phys.* **93,** 7543 (1990).
39. S. Hafner and H. W. Spiess, Multiple-pulse line narrowing under fast magic angle spinning, *J. Magn. Reson. A* **121,** 160 (1996).
40. M. Hohwy and N. C. Nielsen, Elimination of high order terms in multiple pulse nuclear magnetic resonance spectroscopy: Application to homonuclear decoupling in solid, *J. Chem. Phys.* **106,** 7571 (1997).
41. M. Hohwy, P. V. Bower, H. J. Jakobsen, and N. C. Nielsen, A high-order and broadband CRAMPS experiment using z-rotational decoupling, *Chem. Phys. Lett.* **273,** 297 (1997).
42. C. P. Slichter, "Principles of Magnetic Resonance," 3rd ed., Springer-Verlag, New York (1990).
43. R. R. Ernst, G. Bodenhausen, and A. Wokaun, "Principles of Nuclear Magnetic Resonance in One and Two Dimensions," Clarendon Press, Oxford (1987).
44. S. Smith, T. Levante, B. H. Meier, and R. R. Ernst, Computer simulations in magnetic resonance: An object oriented programming approach, *J. Magn. Reson. A* **106,** 75 (1994).
45. D. P. Burum and W.-K. Rhim, Proton NMR study of gypsum, $CaSO_4 \cdot 2H_2O$, using an improved technique for homonuclear dipolar decoupling in solids, *J. Magn. Reson.* **34,** 241 (1979).
46. D. P. Burum, M. Linder, and R. R. Ernst, A new "tune-up" NMR

pulse cycle for minimizing and characterizing phase transients, *J. Magn. Reson.* **43,** 463 (1981).

47. D. P. Burum, Combined rotation and multiple pulse spectroscopy (CRAMPS), *Concepts Magn. Reson.* **2,** 213 (1990).

48. R. Tycko, Zero field nuclear magnetic resonance in high field, *J. Chem. Phys.* **92,** 5776 (1990).

49. M. H. Levitt and R. Freeman, Composite pulse decoupling, *J. Magn. Reson.* **43,** 502 (1981).

50. M. H. Levitt, R. Freeman, and T. Frenkiel, Broadband heteronuclear decoupling, *J. Magn. Reson.* **47,** 328 (1982).

51. M. H. Levitt, R. Freeman, and T. Frenkiel, *in* "Advances in Magnetic Resonance" (J. S. Waugh, Ed.), Vol. 12, p. 47, Academic Press, New York (1982).

52. B. Schnabel, U. Haubenreisser, G. Scheler, and R. Mueller, *in* "Proceedings, 19th Congress Ampere, Heidelberg, 1976" (H. Brunner, K. H. Hausser, and D. Schweitzer, Eds.).

53. R. E. Taylor, R. G. Pembleton, L. M. Ryan, and B. C. Gerstein, Combined multiple pulse NMR and sample spinning: Recovery of ^{1}H chemical shift tensors, *J. Chem. Phys.* **71,** 4541 (1979).

54. J. S. Waugh, Uncoupling of local field spectra in nuclear magnetic resonance: Determination of atomic positions in solids, *Proc. Natl. Acad. Sci. USA* **73,** 1394 (1976).

55. P. Caravatti, G. Bodenhausen, and R. R. Ernst, Heteronuclear solid-state correlation spectroscopy, *Chem. Phys. Lett.* **89,** 363 (1982).

56. P. Caravatti, L. Braunschweiler, and R. R. Ernst, Heteronuclear correlation spectroscopy in rotating solids, *Chem. Phys. Lett.* **100,** 305 (1983).

57. D. P. Burum and A. Bielecki, An improved experiment for heteronuclear-correlation 2D NMR in solids, *J. Magn. Reson.* **94,** 645 (1991).

58. N. Schuff and U. Haeberlen, 2D correlation spectroscopy in homonuclear dipolar-coupled solids, *J. Magn. Reson.* **52,** 267 (1983).

59. W. P. Aue, E. Bartholdi, and R. R. Ernst, Two-dimensional spectroscopy. Application to nuclear magnetic resonance, *J. Chem. Phys.* **64,** 2229 (1976).

60. (*a*) G. Bodenhausen, *Prog. NMR Spectrosc.* **14,** 137 (1981); (*b*) D. P. Weitekamp, *in* "Advances in Magnetic Resonance" (J. S. Waugh, Ed.), Vol. 11, Academic Press, New York (1983); (*c*) M. G. Munowitz and A. Pines, *in* "Advances in Chemical Physics" (I. Prigogine and S. A. Rice, Eds.), Vol. 66, Wiley–Interscience, New York (1987).

61. A. J. Shaka and J. Keeler, *Prog. NMR Spectrosc.* **19,** 47 (1986).

62. H. Cho, S. Pfenninger, J. Forrer, and A. Schweiger, Radio-frequency-driven electron-spin-echo-envelope-modulation spectroscopy, *Chem. Phys. Lett.* **180,** 198 (1991).

63. M. E. Tinkham, "Group Theory and Quantum Mechanics," McGraw–Hill, New York (1964).